


# Structural characterization of the thermal unfolding pathway of human VEGFR1 D2 domain

Donatella Diana<sup>1</sup>, Rossella Di Stasi<sup>1</sup>, Sara García-Viñuales<sup>2</sup>, Lucia De Rosa<sup>1</sup>, Carla Isernia<sup>3</sup>, Gaetano Malgieri<sup>3</sup>, Danilo Milardi<sup>2</sup>, Luca D. D'Andrea<sup>4</sup> and Roberto Fattorusso<sup>3</sup> 

<sup>1</sup> Istituto di Biostrutture e Bioimmagini, CNR, Napoli, Italy

<sup>2</sup> Istituto di Cristallografia, CNR, Catania, Italy

<sup>3</sup> Dipartimento di Scienze e Tecnologie Ambientali, Biologiche e Farmaceutiche (DiSTABiF), Università degli Studi della Campania 'Luigi Vanvitelli', Caserta, Italy

<sup>4</sup> Istituto di Scienze e Tecnologie Chimiche 'Giulio Natta', CNR, Milano, Italy

## Keywords

disulfide bond; DSC; NMR; thermal unfolding; VEGF

## Correspondence

R. Fattorusso, Dipartimento di Scienze e Tecnologie Ambientali, Biologiche e Farmaceutiche (DiSTABiF), Università degli Studi della Campania 'Luigi Vanvitelli', Via Vivaldi 43, 81100, Caserta, Italy  
 Tel: +39 0823274637  
 E-mail: roberto.fattorusso@unicampania.it

(Received 6 July 2021, revised 13 October 2021, accepted 21 October 2021)

doi:10.1111/febs.16246

Folding stability is a crucial feature of protein evolution and is essential for protein functions. Thus, the comprehension of protein folding mechanisms represents an important complement to protein structure and function, crucial to determine the structural basis of protein misfolding. In this context, thermal unfolding studies represent a useful tool to get a molecular description of the conformational transitions governing the folding/unfolding equilibrium of a given protein. Here, we report the thermal folding/unfolding pathway of VEGFR1D2, a member of the immunoglobulin superfamily by means of a high-resolution thermodynamic approach that combines differential scanning calorimetry with atomic-level unfolding monitored by NMR. We show how VEGFR1D2 folding is driven by an oxidatively induced disulfide pairing: the key event in the achievement of its functional structure is the formation of a small hydrophobic core that surrounds a disulfide bridge. Such a 'folding nucleus' induces the cooperative transition to the properly folded conformation supporting the hypothesis that a disulfide bond can act as a folding nucleus that eases the folding process.

## Introduction

Vascular endothelial growth factor (VEGF) and its receptors are key regulators of angiogenesis, promoting normal embryonic development through the proliferation and differentiation of endothelial cells (ECs). In healthy adults, angiogenesis is finely tuned by pro- and antiangiogenic factors. Dysregulation of this equilibrium is associated with the onset of pathological conditions, such as diabetic retinopathy, rheumatoid arthritis, and tumor growth [1,2].

VEGF regulates blood and lymphatic vessel development and homeostasis by binding to and activating the three members of the vascular endothelial growth factor (VEGFR) family of tyrosine kinases receptors (TKRs): VEGFR1, VEGFR2, and VEGFR3 [3].

VEGFR1 and VEGFR2 are highly homologous and belong to the platelet-derived growth factor (PDGF) receptor family [4]. The receptors are organized in an extracellular ligand-binding region consisting of seven extracellular immunoglobulin-like (Ig) domains, a short transmembrane region and an intracellular region that includes a tyrosine kinase domain with a large insertion in the middle of the kinase region [5].

Despite the overall architectural similarity, VEGFR1 and VEGFR2 differ significantly in their functional properties. Moreover, the VEGF binding affinity for VEGFR1 ( $K_d \approx 10$  pM) is 10-fold higher than that for kinase insert domain receptor (KDR;  $K_d \approx 100$  pM);

## Abbreviations

CSP, chemical shift perturbation; DTT, Dithiothreitol; ER, endoplasmic reticulum; KDR, kinase insert domain receptor; TCEP, Tris(carboxyethyl)phosphine; TKR, tyrosine kinases receptors; VEGF, vascular endothelial growth factor; VEGFR, vascular endothelial growth factor receptor.

unlike VEGFR2, VEGFR1 also serves as a high-affinity receptor for placenta growth factor (PlGF) [6].

VEGFR2 undergoes strong ligand-dependent tyrosine phosphorylation in intact cells, while VEGFR1 has a weak or undetectable response [5,7–8]. Likewise, the VEGF-dependent mitogenic response exhibited by cells expressing KDR is completely absent in those expressing only VEGFR1 [8]. Domain deletion studies have shown that the second extracellular domain of VEGFR1 (VEGFR1D2) is both necessary [9,10] and sufficient [11] for high-affinity VEGF binding.

The structure of VEGFR1D2 in complex with VEGF revealed that VEGFR1D2 is a member of the immunoglobulin superfamily and can be structurally classified as a member of the I-set [12] despite having sequence differences at 6 of the 20 key I-set positions [11].

Normally, proteins that are translocated to cell membrane surface to serve as receptors are processed by the endoplasmic reticulum (ER). ER-mediated protein maturation includes glycosylation and disulfide bond formation [13]. Glycosylation is an oxygen-independent process [14]. By contrast, disulfide bond formation results from a net oxidation reaction [15]. Remarkably, albeit low levels of oxygen (hypoxia) are known to regulate VEGF expression via translational and transcriptional pathways, we are still far from a detailed knowledge of the role of oxygen and disulfide bond in the protein structure and stability [16].

Structural characterization of protein thermal unfolding represents a fundamental step to describe their folding/unfolding equilibria, which allow to get a more complete description of protein structure and maturation. In the last years, NMR methodologies, combined with CD spectroscopy and DSC analysis, have been exploited to unveil unfolding mechanisms of VEGF mimicking peptides [17,18], metal-binding proteins, and prion proteins [19,20].

In this study, we have investigated at atomic resolution the thermal folding/unfolding pathway of VEGFR1D2 by means of DSC and NMR studies. Indeed, the atomic resolution offered by multidimensional NMR experiments provides an intrinsic multiprobe approach to assess the degree of protein folding cooperativity [18–21], which is otherwise difficult to characterize.

## Results

### DSC measurements

DSC measurements of VEGFR1D2 are reported in Fig. 1. Two heating/cooling cycles have been carried out to determine the reversibility of the process. For

the first heating (Fig. 1A), the obtained thermogram may be deconvoluted into two components (Fig. 1B).

The first component corresponds to a partially reversible endothermic process (85% of reversibility) centered at about 327 K. This first peak may be fitted by a two-state model, characterized by a van't Hoff to calorimetric enthalpy ratio ( $\Delta H_{\text{vH}}/\Delta H_{\text{cal}}$ ) of  $1.00 \pm 0.02$  and by an enthalpy of the process of  $198 \pm 2 \text{ kJ}\cdot\text{mol}^{-1}$  (Table 1).

The second endothermic transition is centered at about 340 K; in this case, the two-state formalism is not applicable because the calculated van't Hoff to calorimetric enthalpy ratio ( $\Delta H^{\text{vH}}/\Delta H^{\text{cal}}$ ) is far from the unity.

In a reheating run (Fig. 1), this second thermal transition occurs at higher temperature ( $T_m = 347 \text{ K}$ ) and is characterized by a bit larger enthalpy ( $39 \pm 1 \text{ kJ}\cdot\text{mol}^{-1}$ ) with respect to that observed in the first scan; the increase in the enthalpy of the second component after the first heating/cooling cycle coupled with the observed partial reversibility of the first transition suggests that part of the protein does not fold back to its native state.

### Disulfide bond stability upon thermal unfolding

Many studies suggest that intramolecular disulfide linkages are important structural elements that significantly contribute to the thermodynamic stability of globular proteins [22]. However, the exact mechanism by which the disulfide bridge may stabilize proteins remains elusive because it may affect both enthalpy and entropy of native and unfolded states as well. It has been estimated that the entropic contribution of the disulfide bridge is roughly related to the number of residues in the loop connecting the two cysteines according to the following equation [23]:

$$\Delta S_{\text{SS-}} = 8.8 + 1.5 R \ln(N_{\text{res}}) \text{ J}\cdot\text{K}^{-1}\cdot\text{Mol}^{-1}$$

where  $N_{\text{res}}$  is the number of residues in the SS loop and  $R$  is the universal gas constant. For VEGFR1D2, the disulfide bridge links the two cysteines Cys158 e Cys207, so that  $N_{\text{res}} = 47$  with an estimated  $\Delta S_{\text{SS-}} = 54.05 \text{ J}\cdot\text{K}^{-1}\cdot\text{Mol}^{-1}$ . This value approximately corresponds to the entropy change associated with the second transition:  $\Delta S = \Delta H/T = 15/339.87 = 44.13 \text{ J}\cdot\text{K}^{-1}\cdot\text{Mol}^{-1}$  consistent with the hypothesis that formation of the disulfide bridge may seed further folding of polypeptide chain into the native structure. To check the integrity of the disulfide bond at high temperature (Figs 2A–C and 3A,B), protein VEGFR1D2 was incubated at 353 K for 40 min, reacted with iodoacetamide and analyzed by mass spectrometry. Alkylation of

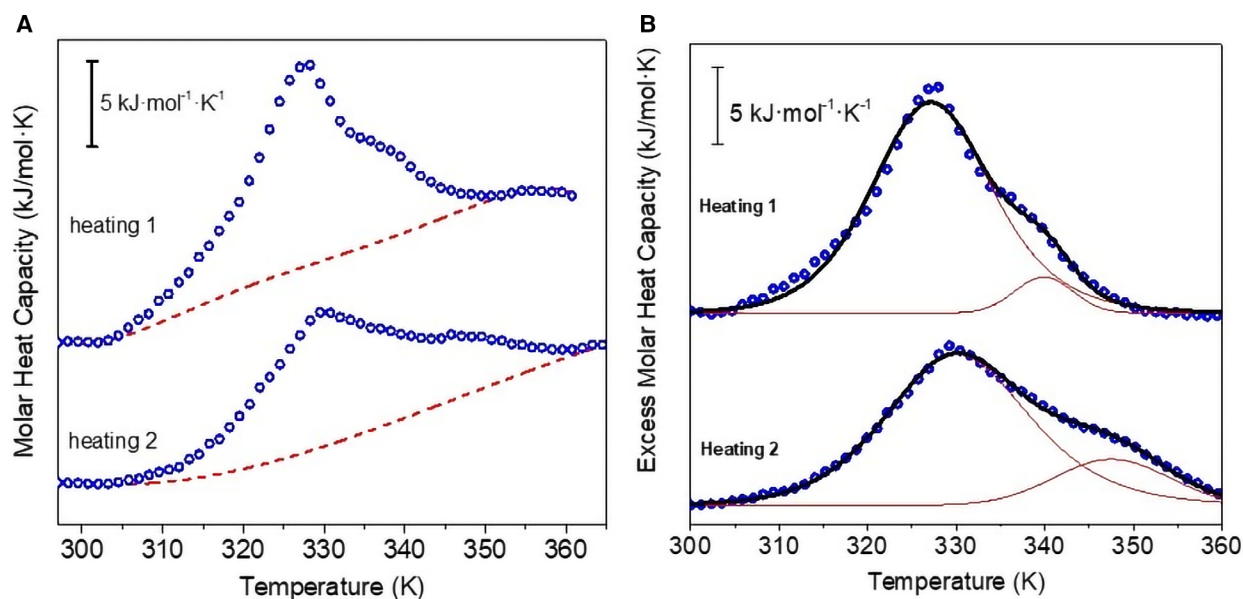


**Fig. 1.** (A) Heat capacity curves of 35  $\mu\text{M}$  VEGFR1D2 in buffer (20 mM Tris-HCl, pH = 7.0, 120 mM NaCl) heating rate 1  $\text{K}\cdot\text{min}^{-1}$  (blue circles). Red dashed lines represent baselines estimated as reported in the text. (B) Excess molar heat capacity curves of VEGFR1D2 obtained from the calorimetric scans shown in the left panel. Blue circles, black lines, and red lines represent the experimental data, the obtained fits are their deconvoluted components, respectively.

**Table 1.** Melting temperatures ( $T_m$ ) and enthalpies ( $\Delta H$ ) of the thermal transitions of VEGFR1D2.

1st heating		2nd heating	
$T_m$ (K)	$\Delta H$ (KJ·mol <sup>-1</sup> )	$T_m$ (K)	$\Delta H$ (KJ·mol <sup>-1</sup> )
327.36 $\pm$ 0.08	198 $\pm$ 2	330.37 $\pm$ 0.1	168 $\pm$ 2
339.87 $\pm$ 0.02	15 $\pm$ 2	347.5 $\pm$ 0.2	39 $\pm$ 1

cysteine residues gave information on the stability of the disulfide bridge.

The analysis of the mass spectra revealed that the disulfide bond in VEGFR1D2 upon thermal unfolding is still intact (Fig. 2A–C). In fact, the molecular mass of the heated protein (MW = 11851.787 Da, Fig. 2B) corresponds to that of the intact native domain (MW = 11851.886 Da, Fig. 2A). As control, a sample of VEGFR1D2 was reduced with DTT, incubated at 353 K, and then with iodoacetamide. In this case, the mass spectrum clearly shows the presence of the double alkylated protein (MW = 11910.914 Da and 11968.022 Da, Fig. 2C).

### NMR thermal unfolding

A virtually complete  $H_N$  and  $^{15}\text{N}$  resonance assignment of VEGFR1D2 was achieved on the basis of

previously reported chemical shift data [24]. The thermal unfolding mechanism of VEGFR1D2 has been therefore investigated at atomic resolution by acquiring a series of 2D [ $^1\text{H}$ ,  $^{15}\text{N}$ ] HSQC spectra as function of the temperature, between 293 K and 353 K at intervals of 5 K.

The NMR thermal analysis shows that  $^1\text{H}$ ,  $^{15}\text{N}$  resonances of VEGFR1D2 exhibited continuous chemical shift variations in the 293–323 K range and most of them still preserve a good spectral dispersion at 323 K as showed in Fig. 4A,B.

Larger chemical shift perturbations (CSP), reported as  $\Delta\delta_{\text{HN}}$ , are observed at the N and C termini, with values higher than mean values plus the standard deviation (Fig. 5A). Significant  $\Delta\delta_{\text{HN}}$  is also observed in many of the loops connecting the secondary structure elements, whose backbone amide groups appear to be very slightly affected by the 30 K temperature increase (Fig. 5B). In the same temperature range, most of the residues experience also an intensity reduction, reported in Fig. 5C and mapped on the protein surface in Fig. 5D.

Interestingly, opposite to the CSP behavior, the residues affected by the most pronounced intensity reductions are included in the seven  $\beta$ -strands forming the  $\beta$ -barrel. Upon further temperature increase, all the cross-peaks completely disappear at 333 K and then reappear at 343 K with a significantly reduced

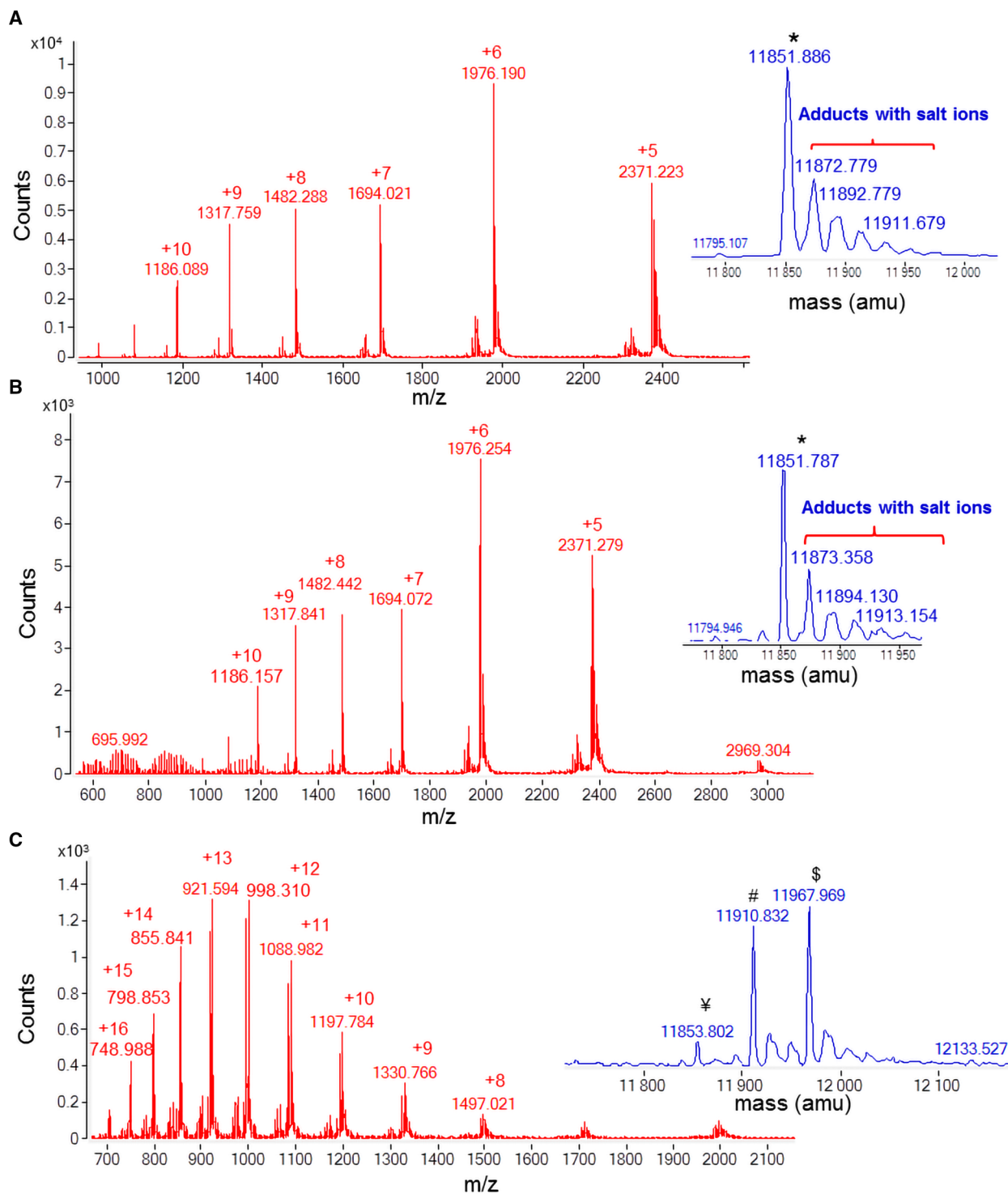
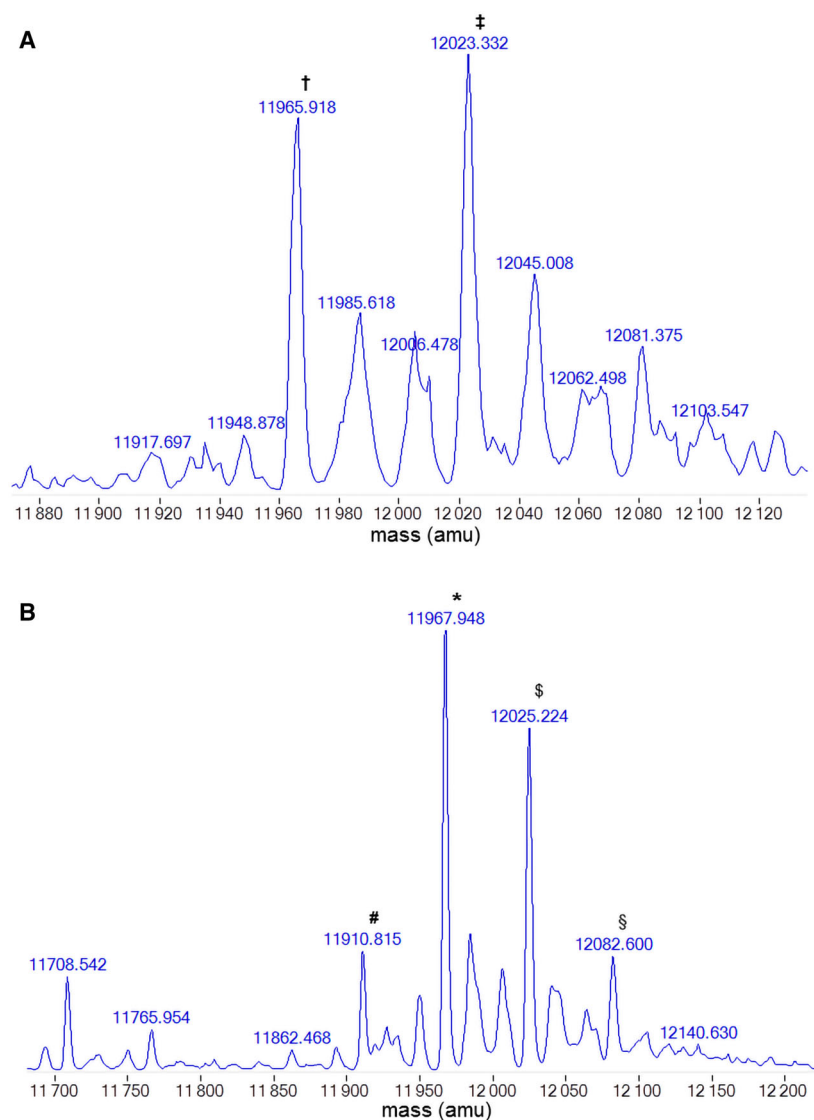


**Fig. 2.** (A) ESI-ToF MS analysis of VEGFR1D2 alkylated at room temperature (RT) after incubation at 353 K in presence and absence of DTT. (B) Untreated VEGFR1D2; (B) VEGFR1D2 treated at 353 K for 40 min and alkylated with iodoacetamide at RT for 30 min; and (C) VEGFR1D2 treated at 353 K for 40 min in presence of DTT and alkylated with iodoacetamide at RT for 30 min. In the insets are reported the deconvoluted mass spectra showing the experimental average mass values of the species. VEGFR1D2 (\*),  $MW_{th}$  (av): 11851.688 Da; reduced VEGFR1D2 (¥),  $MW_{th}$  (av): 11853.688; monoalkylated VEGFR1D2 (#),  $MW_{th}$  (av): 11910.738 Da; dialkylated VEGFR1D2 (\$),  $MW_{th}$  (av): 11967.788 Da.

**Fig. 3.** ToF MS analysis of VEGFR1D2 incubated and alkylated at 353 K, in presence and absence of DTT. (A) Deconvoluted ESI-ToF mass spectrum of VEGFR1D2 treated at 353 K for 40 min and alkylated at 353 K for 30 min with iodoacetamide. (†): VEGFR1D2 with the intact disulfide bridge and unspecifically dialkylated on residues other than Cys ( $MW_{th}$  (av): 11965.788 Da); (‡): VEGFR1D2 unspecifically trialkylated on residues other than Cys ( $MW_{th}$  (av): 12022.838 Da). (B) Deconvoluted ESI-ToF mass spectrum of VEGFR1D2 treated at 353 K for 40 min in presence of DTT and alkylated with iodoacetamide at 353 K for 30 min. (#): VEGFR1D2 with reduced cysteines and monoalkylated ( $MW_{th}$  (av): 11910.738 Da); (\*): VEGFR1D2 with reduced cysteines and dialkylated ( $MW_{th}$  (av): 11967.788 Da); (§): VEGFR1D2 with reduced cysteines and trialkylated ( $MW_{th}$  (av): 12024.838 Da); (§§): VEGFR1D2 with reduced cysteines and tetralkylated ( $MW_{th}$  (av): 12081.888 Da).



chemical shift spread of the signals, which indicates that the protein has undergone a complete thermal unfolding (Fig. 4B). This spectroscopic behavior suggests that the transition occurring in 323–343 K range is characterized by a cooperative thermal unfolding in which the folded VEGFR1D2 structure exchanges with the unfolded conformation in the micro-millisecond timescale [21,25,26]. Refolding experiments were monitored either starting from 333 and from 353 K and denaturation has been found to be almost completely reversible if the sample is heated up to 333 K but the extent of reversibility decreases when the protein is exposed to higher temperature. Indeed, as showed in Fig. 4B, VEGFR1D2 does not refold at all to the native state when heated to 353 K.

### Disulfide bond reduction

In order to underline the importance of the oxidatively induced disulfide pairing, VEGFR1D2 (20  $\mu$ M) was incubated in the presence of 5 mM or 10 mM of the reducing agent tris(carboxyethyl)phosphine (TCEP) at pH = 7. All the reactions were monitored by means of LC-MS as reported in Materials and Methods. TCEP at 5 mM concentration resulted ineffective to completely reduce VEGFR1D2 disulfide bond, also after an incubation time of 24 h at room temperature. The incubation with 10 mM TCEP resulted in about 60% of reduced protein after 5 h of incubation. Prolonging the incubation with 10 mM TCEP to 24 h, the protein underwent a strong destabilization as it

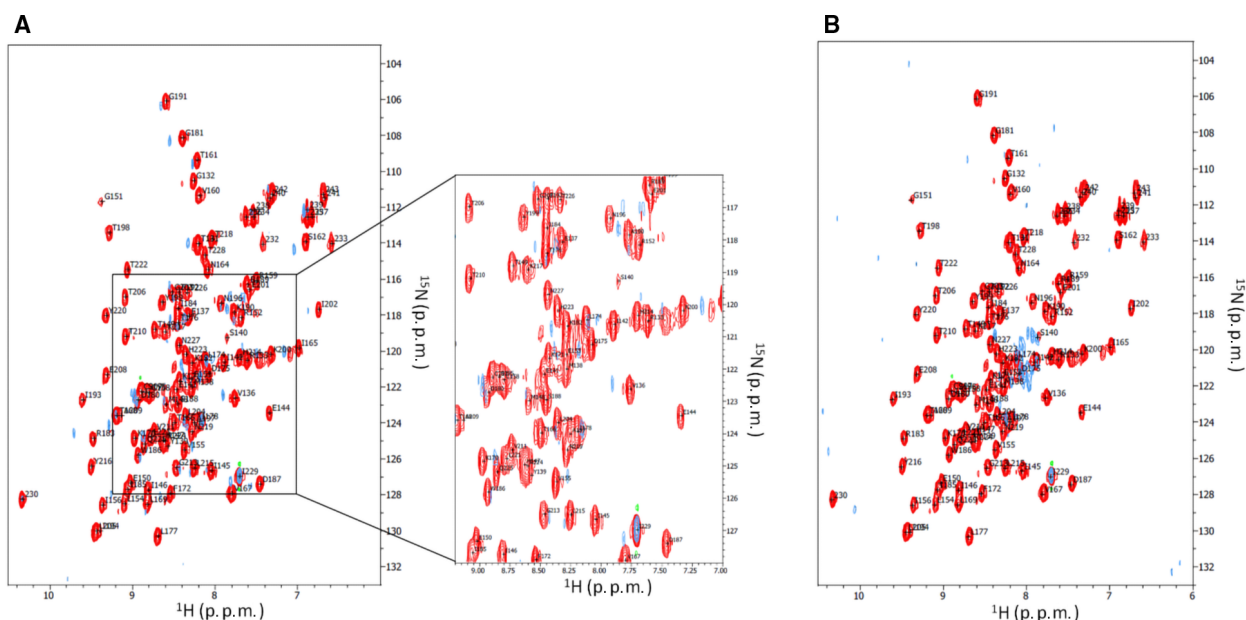


**Fig. 4.** (A) Overlay of  $[^1\text{H}-^{15}\text{N}]$  HSQC spectra of VEGFR1D2 up to the last temperature (323 K) at which the signals are observed; (B) Overlay of 2D  $[^1\text{H}, ^{15}\text{N}]$  HSQC spectra of VEGFR1D2 at 298 K (red) and 353 K (blue).

resulted entirely precipitated in the reaction tube. Mass spectrometry analysis performed on the resuspended pellet showed the presence of a completely reduced protein domain (Fig. 6A,B). The molecular weight (MWth (av)) of VEGFR1D2 with disulfide-bonded cysteines resulted 11851.688 Da (Fig. 6B) while the MWth (av) of VEGFR1D2 with reduced cysteines was 11853.688 Da (Fig. 6A).

VEGFR1D2 precipitation after 24 h incubation with 10 mM TCEP hindered CD measurements or NMR analyses of the reduced protein but, at the same time, was indicative of a strong destabilization of the VEGFR1D2. This result supports our hypothesis based on the assumption of a protein folding mechanism for VEGFR1D2 driven by the formation of domain disulfide bridge.

## Discussion

The comprehension of the folding mechanisms at the basis of protein and structure functions appears crucial to determine structural bases of protein misfolding [27]. Thermal unfolding studies may be very useful to get a molecular description of the conformational transitions governing the folding/unfolding equilibrium of a given protein [28]. Multinuclear NMR methodologies, coupled with DSC analysis, represent a powerful tool to describe protein thermal unfolding mechanisms at an atomic level [20,29–33]. The human VEGFR1D2 is an Ig domain of the I-set containing one small  $\beta$ -sheet

involving strands B, E, and D, a second larger  $\beta$ -sheet involving strands A', G, F, C, and C', and a short helical turn consisting of residues 199–201 in the crossover between strands E and F (Fig. 5) and a disulfide bridge links Cys158 with Cys207. Four residues at both the N- and C-terminal ends are disordered, whereas the 40 residues in the  $\beta$ -strands are well defined [24]. VEGFR1D2 faces VEGF with the 'bottom' half of its five-stranded sheet, a surface made up of residues from the N-terminal bulge, strand A', part of strands G and F, the loop connecting strands C and C', and the helical turn connecting strands E and F.

Previously, we reported VEGFR1D2 CD thermal unfolding showing a sigmoidal transition with a melting temperature of 333 K. Now, we can add more molecular details to VEGFR1D2 thermal unfolding picture. In fact, NMR and DSC data clearly indicate that VEGFR1D2 thermal unfolding can be divided into three parts upon temperature increase: a first small increase in the structural disorder, between 298 and 323 K, preceding a second structural transitions between 323 and 343, corresponding to a classical cooperative two-state unfolding and a third transition, detected by the DSC analysis, very likely attributable to the definitive unfolding of the loop connecting the Cys158–Cys207 disulfide bridge.

The atomic resolution NMR analysis shows how, during the first preparative conformational modification, VEGFR1D2 residues behave in two distinct manners. Those included in the most flexible regions, more

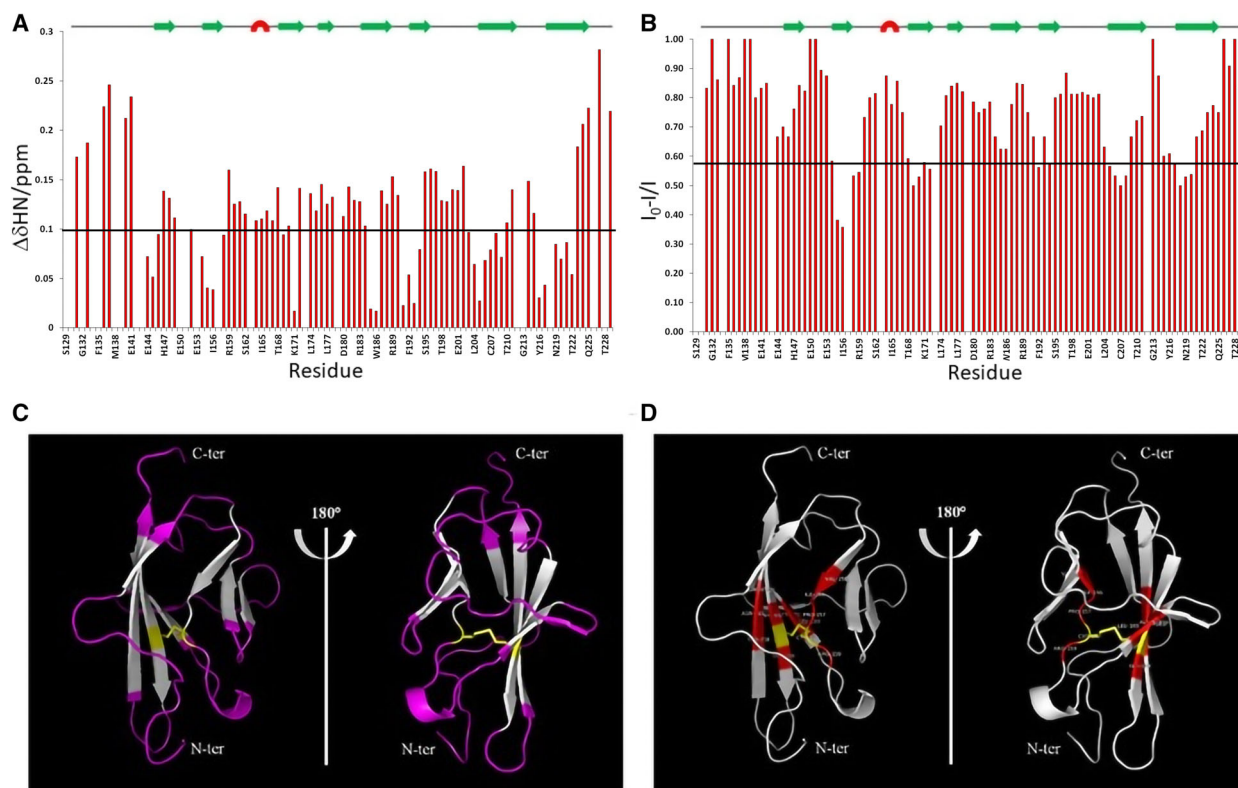


**Fig. 5.** (A) Bar graphs of the average combined chemical shift differences ( $\Delta\text{HN}_{\text{av}}$ ) as a function of residue number. The mean value (plus the standard deviation) ( $\Delta\text{HN}_{\text{av}} = 0.10$  ppm) is shown as a continuous line. The secondary structure elements are also indicated. (B) CSP mapping onto the representative conformer of the NMR structure of VEGFR1D2 shown as ribbon drawing. Residues for which  $\Delta\text{HN}_{\text{av}} > 0.10$  ppm are shown in magenta. Disulfide bridge between C158 and C207 is highlighted in yellow. (C) Bar graphs of the intensity difference ( $I_0 - I$ ) as a function of residue number. The mean value ( $I_0 - I = 0.55$  ppm) is shown as a broken line. The secondary structure elements are also indicated. (D) Intensity difference mapping onto the representative conformer of the NMR structure of VEGFR1D2 shown as ribbon drawing. Residues for which  $I_0 - I > 0.55$  ppm are shown in red. Disulfide bridge between C158 and C207 is highlighted in yellow. Structures figures were created with the program Pymol.

particularly at the N- and C-terminal ends, the loops connecting the seven  $\beta$ -strands and the small helical turn, experience a sensible CSP and a more reduced signal intensity reduction. These NMR parameter variations indicate fast conformational exchanges, which, upon temperature increase, tend toward less structured conformations. Conversely, protein residues affected by much smaller CSPs and more significant signal intensity reductions are all included in the more structured VEGFR1D2 regions (Fig. 5). Significant reductions in signal intensity unveil intermediate conformational exchanges between well-structured and much less structured conformations. Particularly, the residues affected by a significant signal intensity, i.e., lower than the average values minus the standard deviation (i.e.,  $\Delta I < 0.7$ ), are comprised in all the seven  $\beta$ -strands and the loop containing Cys158, which follows B strand (Fig. 5C). Whether the residues affected by the largest intensity reductions, having  $\Delta I < 0.55$ , are considered, a small hydrophobic core including

the disulfide bridge is defined (Fig. 5D). This hydrophobic core, in intermediate exchange with structured VEGFR1D2 conformation at 323 K, reasonably represents the smallest protein nucleus able to induce the cooperative transition from the unfolded VEGFR1D2 structure to the properly folded functional conformation. Accordingly, the estimated entropic contribution for the structural transition of the disulfide bridge region in large part corresponds to the entropy change associated with the second DSC transition further suggesting the presence of the disulfide bridge as a seed for the complete folding of VEGFR1-D2 into the native structure.

Globally, the thermal folding/unfolding mechanism of VEGFR1D2, here determined, can be described as it follows. The folding of the loop included within the two cysteines forming the disulfide bridge, centered at around 347 K, precedes the formation of a small hydrophobic core that surrounds the bridge (Fig. 5D). It acts as a ‘folding nucleus’ [34,35], which then enlarges

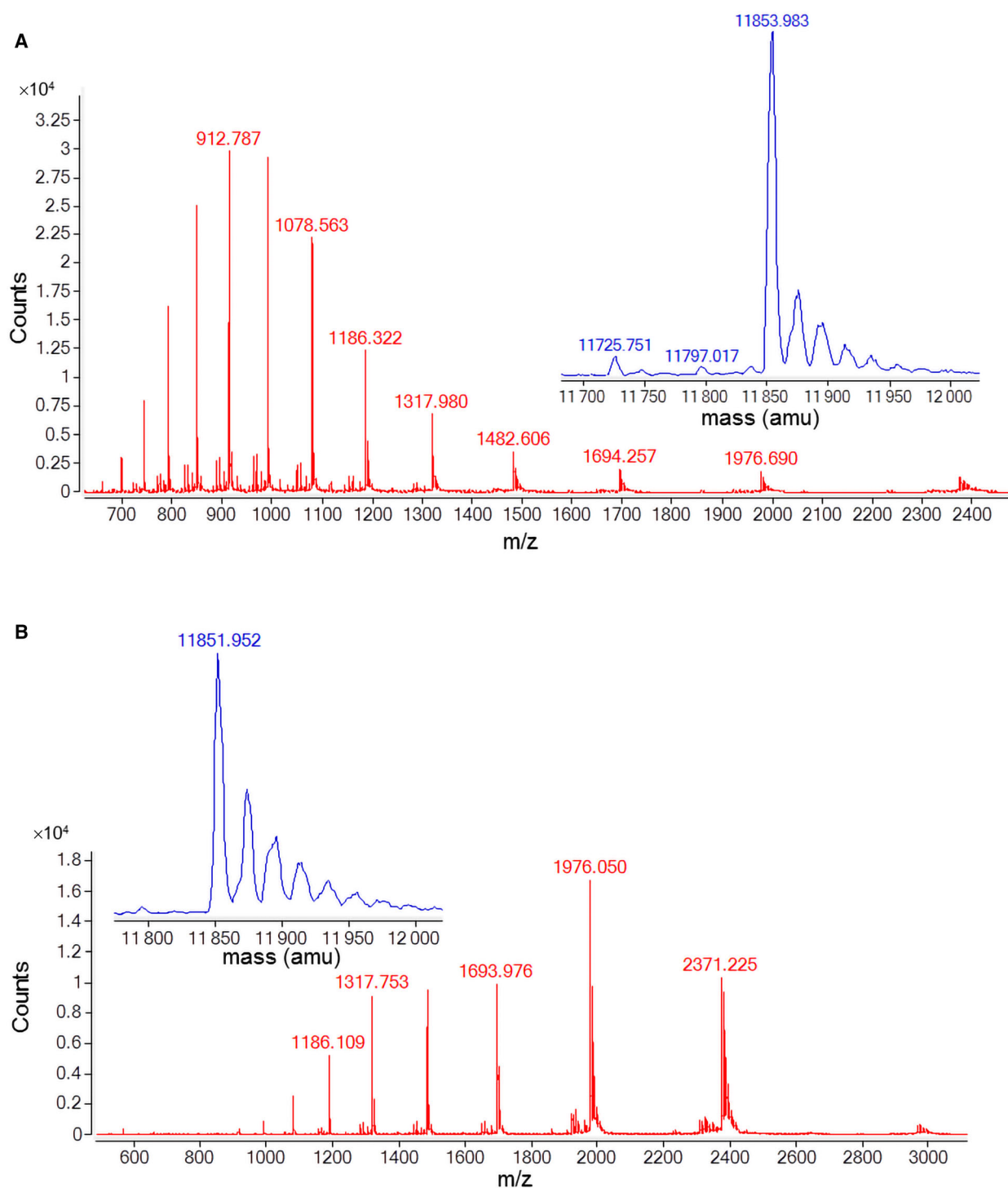


**Fig. 6.** ESI-ToF MS analysis of VEGFR1D2. (A) VEGFR1D2 (20  $\mu\text{M}$ ) was incubated in 20 mM phosphate buffer, 10 mM TCEP, pH 7.0, for 24 h at room temperature. The protein solution was centrifuged and the insoluble fraction was solubilized with 8 M guanidinium hydrochloride and analyzed by LC-MS ESI ToF. The mass spectrum of the protein peak is reported; the inset shows the deconvoluted mass spectrum. For comparison, the mass spectrum of VEGFR1D2 is also reported (B).



comprising the residues included in the seven  $\beta$ -strands (Fig. 5D); at 323 K the collapse of VEGFR1D2 native fold occurs. Successively, between 323 and 298 K, the residues comprised at the N and C termini and in the loop connecting the secondary structure elements further change their conformation, reaching the protein native state at room temperature. Overall, the folding mechanism of the oxidized VEGFR1D2 domain can be inserted in the 'nucleation-condensation' category [35], which is between the conformational selection and induced-fit mechanisms. Interestingly, the bottom half of VEGFR1D2, which represents the binding surface to VEGF, is constituted by a major portion which contribute to the cooperative transition and a minor more flexible part constituted by residues which do not directly participate in the protein folding and appear to guarantee a certain degree of conformational flexibility.

Next, we can also argue that folding of VEGFR1D2 may be considered a hierarchic process where global folding is ignited by small-sized local structures (e.g., the disulfide bridge) that interact to generate intermediate states of increasing complexity leading, ultimately, to the native structure [36]. Intriguingly, there are other known examples (e.g., insulin and proinsulin) where protein folding is driven by an oxidatively induced disulfide pairing [37], thus supporting the hypothesis that a disulfide bond can act as folding nucleus and ease the folding process [38].

Folding stability represents a key feature of protein evolution and is fundamental for their functional roles. At this regard, NMR spectroscopy coupled with DSC and possibly also with CD spectroscopy can give detailed information about thermal unfolding mechanisms of small globular domains, also when based on a cooperative two-state transition. In this study, we show that analysis of CSPs and intensity reductions upon protein thermal unfolding provides important insights of cooperative folding transition and has been rarely reported in the past. Expanding such studies to the majority of the protein structure determined via NMR spectroscopy would provide a crucial survey of the conformational equilibria governing protein structure, functions, and evolution.

## Materials and methods

### *E. coli* expression, refolding, and purification of VEGFR1D2

The uniformly labeled  $^{15}\text{N}$ -VEGFR1D2 was expressed, refolded, and purified as previously described [39]. Briefly, DNA fragment corresponding to VEGFR1D2 gene

(encoding amino acids 129–229 of the human VEGFR1 gene) was amplified by PCR reaction starting from the cDNA of the full receptor and cloned into the *NcoI*/*XhoI* sites of pETM11 expression vector (Novagen, Podenzano, Italy), downstream to the His-tag and TEV recognition site sequences. The recombinant construct was expressed in *E. coli* BL21 *Codon Plus* (DE3) RIL cell strain (Agilent Technologies-Stratagene, Santa Clara, CA, USA). Bacterial expression was carried out according to Sambrook *et al.* [40] (in 1 L of pre-warmed minimal medium containing  $^{15}\text{NH}_4\text{Cl}$  ( $1\text{ g}\cdot\text{L}^{-1}$ ) as the unique source of nitrogen,  $50\text{ }\mu\text{g}\cdot\text{mL}^{-1}$  kanamycin, and  $33\text{ }\mu\text{g}\cdot\text{mL}^{-1}$  chloramphenicol). Once reached  $0.8\text{ OD}_{600\text{nm}}$ , the culture was induced with  $0.7\text{ mM}$  isopropyl- $\beta$ -D-1-thiogalattopyranoside (IPTG). After 5 h at  $37\text{ }^\circ\text{C}$ , cells were harvested and lysed by sonication in a buffer containing  $50\text{ mM}$  Tris-HCl,  $\text{pH} = 8.0$ , and protease inhibitors cocktail (Roche, Basel, Switzerland). Bacterial lysate was then centrifuged ( $34\,957\text{ g}$ , 30 min, and  $4\text{ }^\circ\text{C}$ ) and the pellet fraction containing  $^{15}\text{N}$ -VEGFR1D2 in inclusion bodies was resuspended in  $50\text{ mM}$  Tris-HCl,  $150\text{ mM}$  NaCl,  $10\text{ mM}$  imidazole,  $8\text{ M}$  urea, and  $\text{pH} = 8.0$  (Buffer A) to solubilize the protein domain. Solubilized His-tagged  $^{15}\text{N}$ -VEGFR1D2 was loaded on Ni(II)-NTA resin and a column refolding was carried out by equilibrating the in-batch resin with the above-mentioned Buffer A containing decreasing concentration of urea. Finally,  $^{15}\text{N}$ -labeled domain was eluted by a step gradient increasing imidazole concentration from  $100$  to  $300\text{ mM}$ . Elutions of His-tagged domain were pooled and dialyzed overnight against  $50\text{ mM}$  Tris-HCl,  $250\text{ mM}$  NaCl,  $3\text{ mM}$  reduced/ $0.3\text{ mM}$  oxidized),  $\text{pH} = 7.0$ , at  $4\text{ }^\circ\text{C}$ . TEV cleavage reaction was performed adding protease to protein substrate in a molar ratio (protease : substrate) of  $1 : 35$ , for 3 h at  $30\text{ }^\circ\text{C}$ . The cleaved  $^{15}\text{N}$ -VEGFR1D2 was concentrated by the Amicon Ultra system ( $10.000\text{ MWCO}$ , Millipore, Burlington, MA, USA) and purified to homogeneity by size exclusion chromatography on a S75 column (GE Healthcare, Milano, Italy) equilibrated with  $20\text{ mM}$  Tris-HCl,  $120\text{ mM}$  NaCl,  $\text{pH} 7.0$ . The purified product was concentrated again until  $0.9\text{ mM}$ .

### Alkylation reaction with iodoacetamide

In order to estimate the oxidation state of the disulfide bridge at  $353\text{ K}$ , VEGFR1D2 was diluted up to  $10\text{ }\mu\text{M}$  in Tris-HCl  $50\text{ mM}$ ,  $\text{pH} = 7.0$ , containing  $150\text{ mM}$  NaCl and incubated for 40 min in a thermostated bath set to the above-mentioned temperature. Then, iodoacetamide (Sigma-Aldrich, St. Louis, MO, USA), dissolved at a concentration of  $500\text{ mM}$  in the same buffer, was added to the heat-treated protein domain at a final concentration of  $14\text{ mM}$ . The alkylation reaction was allowed to proceed at room temperature, for 30 min, in the dark. As positive control, VEGFR1D2 was first reduced with  $5\text{ mM}$  DTT at  $353\text{ K}$  for 40 min and then alkylated by iodoacetamide as described for the

unreduced sample. Analysis of protein samples was assessed by LC-MS on an Agilent 1200 Infinity Series (Agilent Technologies) equipped with an ESI source and a ToF detector, using an Aeris widepore (150 × 2.1 mm, 3.6 μm) XB-C8 column (Phenomenex, Bologna, Italy), applying a method with a flow rate of 0.2 mL·min<sup>-1</sup> and a linear gradient of CH<sub>3</sub>CN (0.05% TFA) in H<sub>2</sub>O (0.05% TFA) from 5% to 70% in 20 min.

### Nuclear magnetic resonance spectroscopy

VEGFR1D2 sample was dissolved in 500 μL of aqueous buffer containing 20 mM Tris-HCl (pH = 7.0) and 120 mM NaCl (10% D2O for the lock) at concentration of 150 μM. All of the NMR spectra were carried out on a Varian Inova 600 MHz spectrometer equipped with cold probe, where the probe temperature was regularly calibrated by using methanol and ethylene glycol [41]. All NMR experiments were processed with SPARKY [42] and analyzed with NEASY, a tool of CARRA software [43]. For the thermal unfolding experiments, a series of bi-dimensional [<sup>1</sup>H-<sup>15</sup>N] HSQC spectra were acquired increasing temperatures at regular intervals of 5 K from 293 to 353 K, recording all the spectra consecutively. Intensity ratios were computed as  $I_0 - I / I_0$ , where  $I_0$  is the signal intensity in the reference spectra at 298 K and  $I$  is the intensity in the spectra acquired at 323 K. The per residue CSP weighted average chemical shift differences, ΔδHN, were calculated for the amide <sup>15</sup>N and <sup>1</sup>H resonances using the following equation:  $\Delta\delta\text{HN} = ((\Delta^1\text{H})^2 + (0.17 \Delta^{15}\text{N})^2)^{1/2}$ , where Δ<sup>1</sup>H and Δ<sup>15</sup>N are the differences between the chemical shifts at 298K and 323K. The color figures and the structure analysis were performed with the programs MOLMOL [44] and Pymol [45].

### Differential scanning calorimetry

A 35 μM VEGFR1D2 in buffer (20 mM Tris-HCl, pH = 7.0, 120 mM NaCl) solution was vacuum degassed and heated at a scan rate of 1 K·min<sup>-1</sup> in the temperature range 283–373 K. An extra external nitrogen pressure of 3 atm was applied to the sample to prevent the formation of air bubbles during heating. The reference cell of the calorimeter was filled with protein-free buffer. To ensure an accurate equilibration of the calorimeter, several buffer–buffer heating scans were routinely performed before any DSC measurement. To obtain the molar heat capacity curves Cp(T), a buffer–buffer baseline was subtracted from raw DSC curves and normalized by the protein concentration as reported elsewhere [46]. For all experiments, two consecutive heating–cooling cycles were performed to determine the reversibility of the process. Excess molar heat capacities curves (Cp<sub>exc</sub>) were obtained from Cp(T), by subtracting a baseline obtained by a third-order polynomial fit of the pre- and post-transition Cp trends. DSC

experiments were performed using a NanoDSC instrument (TA Instruments) and Cp<sub>exc</sub> curves were deconvoluted by the NanoAnalyze software using the two-state or the Gaussian models.

The van't Hoff enthalpy ΔH<sup>VH</sup> can be calculated according to Eqn (1),

$$\Delta H^{\text{VH}} = \frac{4RT_m^2 \Delta C_p(T_m)}{\Delta H_{\text{cal}}} \quad (1)$$

where  $T_m$ ,  $\Delta C_p(T_m)$ , and  $\Delta H_{\text{cal}}$  are the transition temperature, the corresponding excess heat capacity and the calorimetric enthalpy determined from the heat capacity curve. The ratio of the van't Hoff to the calorimetric enthalpy ( $r^{\text{VH}} = \Delta H^{\text{VH}} / \Delta H_{\text{cal}}$ ) is considered as a valuable indicator of the validity of the assumption that protein thermal unfolding may be considered as a 'two state' transition [47].

### Liquid chromatography-mass spectrometry

VEGFR1D2 of 20 μM was incubated in phosphate buffer 20 mM and TCEP 5 or 10 mM, pH = 7. All the reactions were monitored by LC-MS, analyzing protein samples on an Agilent 1200 Infinity Series (Agilent Technologies) equipped with an ESI source and a ToF detector. Protein samples were loaded on an Aeris widepore (150 × 2.1 mm, 3.6 μm) XB-C8 column (Phenomenex), applying a method with a flow rate of 0.2 mL·min<sup>-1</sup> and a linear gradient of CH<sub>3</sub>CN (0.05% TFA) in H<sub>2</sub>O (0.05% TFA) from 5% to 70% in 20 min. The protein sample precipitated after 24 h of incubation with 10 mM TCEP was centrifuged, the pellet was resuspended in 50 μL of 8 M guanidinium hydrochloride and 1.5 μL were also analyzed.

### Acknowledgements

This work was supported by Italian MIUR (grant number 2017WBZFHL). SG acknowledges the European Union Horizon 2020 research and innovation program for funding her Ph.D. fellowship under the Marie Skłodowska-Curie grant agreement INCIPIT n. 665403. Open Access Funding provided by Università degli Studi della Campania Luigi Vanvitelli within the CRUI-CARE Agreement. WOA Institution: Università degli Studi della Campania Luigi Vanvitelli. Blended DEAL: CARE. Open Access Funding provided by Università degli Studi della Campania Luigi Vanvitelli. [Correction added on 24 May 2022, after first online publication CRUI funding statement has been added.]

### Conflicts of interest

The authors declare no conflict of interest.

## Author contributions

DD: acquired and analyzed all the NMR experiments. RDS and LDR: expressed and purified the protein samples; performed and analyzed alkylation and LC-MS experiments. SGV: performed and analyzed DSC experiments. CI, GM, LDDA, and DM: designed the experiments and supervised the study. RF: conceived and designed the study and wrote the manuscript. All the authors revised the manuscript.

## Peer Review

The peer review history for this article is available at <https://publons.com/publon/10.1111/febs.16246>.

## References

- Ferrara N & Davis-Smyth T (1997) The biology of vascular endothelial growth factor. *Endocr Rev* **18**, 4–25.
- Klagsbrun M & D'Amore PA (1996) Vascular endothelial growth factor and its receptors. *Cytokine Growth Factor Rev* **7**, 259–270.
- Olsson AK, Dimberg A, Kreuger J & Claesson-Welsh L (2006) VEGF receptor signalling – in control of vascular function. *Nat Rev Mol Cell Biol* **7**, 359–371.
- van der Geer P, Hunter T & Lindberg RA (1994) Receptor protein-tyrosine kinases and their signal transduction pathways. *Annu Rev Cell Biol* **10**, 251–337.
- de Vries C, Escobedo JA, Ueno H, Houck K, Ferrara N & Williams LT (1992) The fms-like tyrosine kinase, a receptor for vascular endothelial growth factor. *Science* **255**, 989–991.
- Park JE, Chen HH, Winer J, Houck KA & Ferrara N (1994) Placenta growth factor. Potentiation of vascular endothelial growth factor bioactivity, in vitro and in vivo, and high affinity binding to Flt-1 but not to Flk-1/KDR. *J Biol Chem* **269**, 25646–25654.
- Seetharam L, Gotoh N, Maru Y, Neufeld G, Yamaguchi S & Shibuya M (1995) A unique signal transduction from FLT tyrosine kinase, a receptor for vascular endothelial growth factor VEGF. *Oncogene* **10**, 135–147.
- Waltenberger J, Claesson-Welsh L, Siegbahn A, Shibuya M & Heldin CH (1994) Different signal transduction properties of KDR and Flt1, two receptors for vascular endothelial growth factor. *J Biol Chem* **269**, 26988–26995.
- Barleon B, Totzke F, Herzog C, Blanke S, Kremmer E, Siemeister G, Marmé D & Martiny-Baron G (1997) Mapping of the sites for ligand binding and receptor dimerization at the extracellular domain of the vascular endothelial growth factor receptor FLT-1. *J Biol Chem* **272**, 10382–10388.
- Cunningham SA, Waxham MN, Arrate PM & Brock TA (1995) Interaction of the Flt-1 tyrosine kinase receptor with the p85 subunit of phosphatidylinositol 3-kinase. Mapping of a novel site involved in binding. *J Biol Chem* **270**, 20254–20257.
- Wiesmann C, Fuh G, Christinger HW, Eigenbrot C, Wells JA & de Vos AM (1997) Crystal structure at 1.7 Å resolution of VEGF in complex with domain 2 of the Flt-1 receptor. *Cell* **91**, 695–704.
- Harpaz Y & Chothia C (1994) Many of the immunoglobulin superfamily domains in cell adhesion molecules and surface receptors belong to a new structural set which is close to that containing variable domains. *J Mol Biol* **238**, 528–539.
- Braakman I & Hebert DN (2013) Protein folding in the endoplasmic reticulum. *Cold Spring Harb Perspect Biol* **5**, a013201.
- Koritzinsky M, Levitin F, van den Beucken T, Rumantir RA, Harding NJ, Chu KC, Boutros PC, Braakman I & Wouters BG (2013) Two phases of disulfide bond formation have differing requirements for oxygen. *J Cell Biol* **203**, 615–627.
- Bulleid NJ & Ellgaard L (2011) Multiple ways to make disulfides. *Trends Biochem Sci* **36**, 485–492.
- Levitin F, Lee SCES, Hulme S, Rumantir RA, Wong AS, Meester MR & Koritzinsky M (2021) Oxygen-independent disulfide bond formation in VEGF-A and CA9. *J Biol Chem* **296**, 1–13.
- Diana D, Ziacco B, Scarabelli G, Pedone C, Colombo G, D'Andrea LD & Fattorusso R (2010) Structural analysis of a helical peptide unfolding pathway. *Chem Eur J* **16**, 5400–5407.
- Diana D, De Rosa L, Palmieri M, Russomanno A, Russo L, La Rosa C, Milardi D, Colombo G, D'Andrea LD & Fattorusso R (2015) Long range Trp-Trp interaction initiates the folding pathway of a pro-angiogenic  $\beta$ -hairpin peptide. *Sci Rep* **5**, 16651.
- Halskau O Jr, Perez-Jimenez R, Ibarra-Molero B, Underhaug J, Muñoz V, Martinez A & Sanchez-Ruiz JM (2008) Large-scale modulation of thermodynamic protein folding barriers linked to electrostatics. *Proc Natl Acad Sci USA* **105**, 8625–8630.
- Sadqi M, Fushman D & Muñoz V (2006) Atom-by-atom analysis of global downhill protein folding. *Nature* **442**, 317–321.
- Palmieri M, Malgieri G, Russo L, Baglivo I, Esposito S, Netti F, Del Gatto A, de Paola I, Zaccaro L, Pedone PV *et al.* (2013) Structural Zn(II) implies a switch from fully cooperative to partly downhill folding in highly homologous proteins. *J Am Chem Soc* **135**, 5220–5228.
- Guzzi R, Sportelli L, La Rosa C, Milardi D, Grasso D, Verbeet MP & Canters GW (1999) A spectroscopic and calorimetric investigation on the thermal stability of the Cys3Ala/Cys26Ala azurin mutant. *Biophys J* **77**, 1052–1063.
- Pace CN, Grimsley GR, Thomson JA & Barnett BJ (1988) Conformational stability and activity of

- ribonuclease T1 with zero, one, and two intact disulfide bonds. *J Biol Chem* **25**, 11820–11825.
- 24 Starovasnik MA, Christinger HW, Wiesmann C, Champe MA, de Vos AM & Skelton NJ (1999) Solution structure of the VEGF-binding domain of Flt-1: comparison of its free and bound states. *J Mol Biol* **293**, 531–544.
- 25 Fung A, Li P, Godoy-Ruiz R, Sanchez-Ruiz JM & Muñoz V (2008) Expanding the realm of ultrafast protein folding: gpW, a midsize natural single-domain with alpha+beta topology that folds downhill. *J Am Chem Soc* **130**, 7489–7495.
- 26 Godoy-Ruiz R, Henry ER, Kubelka J, Hofrichter J, Muñoz V, Sanchez-Ruiz JM & Eaton WA (2008) Estimating free-energy barrier heights for an ultrafast folding protein from calorimetric and kinetic data. *J Phys Chem B* **112**, 5938–5949.
- 27 Yon JM (2002) Protein folding in the post-genomic era. *J Cell Mol Med* **6**, 307–327.
- 28 Garcia-Mira MM, Sadqi M, Fischer N, Sanchez-Ruiz JM & Muñoz V (2002) Experimental identification of downhill protein folding. *Science* **298**, 2191–2195.
- 29 Sanchez-Ruiz JM (2011) Probing free-energy surfaces with differential scanning calorimetry. *Annu Rev Phys Chem* **62**, 231–255.
- 30 Malgieri G, D'Abrosca G, Pirone L, Toto A, Palmieri M, Russo L, Sciacca MFM, Tatè R, Sivo V, Baglivo I *et al.* (2018) Folding mechanisms steer the amyloid fibril formation propensity of highly homologous proteins. *Chem Sci* **9**, 3290–3298.
- 31 Banach M, Stapor K, Konieczny L, Fabian P & Roterman I (2020) Downhill, ultrafast and fast folding proteins revised. *Int J Mol Sci* **21**, 7632.
- 32 Grazioso R, García-Viñuales S, D'Abrosca G, Baglivo I, Pedone PV, Milardi D, Fattorusso R, Isernia C, Russo L & Malgieri G (2020) The change of conditions does not affect Ros87 downhill folding mechanism. *Sci Rep* **10**, 21067.
- 33 Grazioso R, García-Viñuales S, Russo L, D'Abrosca G, Esposito S, Zaccaro L, Iacovino R, Milardi D, Fattorusso R, Malgieri G *et al.* (2020) Substitution of the native Zn (II) with Cd (II), Co (II) and Ni (II) changes the downhill unfolding mechanism of Ros87 to a completely different scenario. *Int J Mol Sci* **21**, 8285.
- 34 Arai M (2018) Unified understanding of folding and binding mechanisms of globular and intrinsically disordered proteins. *Biophys Rev* **10**, 163–181.
- 35 Fersht AR (1997) Nucleation mechanisms in protein folding. *Curr Opin Struct Biol* **7**, 3–9.
- 36 Baldwin RL & Rose GD (1999) Is protein folding hierarchic? I. Local structure and peptide folding. *Trends Biochem Sci* **24**, 26–33.
- 37 Hua QX, Gozani SN, Chance RE, Hoffmann JA, Frank BH & Weiss MA (1995) Structure of a protein in a kinetic trap. *Nat Struct Biol* **2**, 129–138.
- 38 Mason JM, Bendall DS, Howe CJ & Worrall JA (2012) The role of a disulfide bridge in the stability and folding kinetics of Arabidopsis thaliana cytochrome c (6A). *Biochim Biophys Acta* **1824**, 311–318.
- 39 Di Stasi R, Diana D, Capasso D, Palumbo R, Romanelli A, Pedone C, Fattorusso R & D'Andrea LD (2010) VEGFR1(D2) in drug discovery: expression and molecular characterization. *Biopolymers* **94**, 800–809.
- 40 Sambrook J, Fritsch EF & Maniatis T (1989) Molecular Cloning: A Laboratory Manual, 2nd edn. Cold Spring Harbor Laboratory, Cold Spring Harbor, NY.
- 41 Martin M, Martin G & Delpuech J (1980) Practical NMR Spectroscopy. Hayden, NY.
- 42 Goddard TD & Kneller DG (2003) SPARKY 3. University of California, San Francisco.
- 43 Masse JE & Keller R (2005) AutoLink: automated sequential resonance assignment of biopolymers from NMR data by relative-hypothesis-prioritization-based simulated logic. *J Magn Reson* **174**, 133–151.
- 44 Koradi R, Billeter M & Wüthrich K (1996) MOLMOL: a program for display and analysis of macromolecular structures. *J Mol Graph* **14**, 51–55.
- 45 The PyMOL Molecular Graphics System, Version 2.0 Schrödinger, LLC.
- 46 Guzzi R, Sportelli L, La Rosa C, Milardi D & Grasso D (1998) Solvent isotope effects on azurin thermal unfolding. *J Phys Chem B* **102**, 1021–1028.
- 47 Arena G, Fattorusso R, Grasso G, Grasso GI, Isernia C, Malgieri G, Milardi D & Rizzarelli E (2011) Zinc(II) complexes of ubiquitin: speciation, affinity and binding features. *Chem Eur J* **17**, 11596–11603.